FUTURE SATELLITE SOUNDING TECHNIQUES

W. L. Smith, H.-L. Huang, H. E. Revercomb, A. J. Schreiner, and H. M. Woolf
Cooperative Institute for Meteorological Satellite Studies
Madison, Wisconsin USA

1. ABSTRACT

In this paper, two advances in satellite sounding techniques are discussed. The first advance deals with the analytical formulation of the inverse solution; the second advance addresses the greatly improved vertical resolution and accuracy achieved using high spectral resolution and quasi-continuous infrared radiance spectra. The improved analytical formulation enables the separation of the generally overlapping uniformly mixed gas and water vapor emission components of the radiance signal, thereby providing an exact linearized form of the radiative transfer equation which can be solved for atmospheric temperature and humidity profiles without iteration. Also presented are theoretical and experimental results demonstrating that high spectral resolution and quasi-continuous infrared spectra provide a factor of two or greater improvement in retrieved sounding vertical resolution and accuracy over that achieved with contemporary filter radiometers. The paper concludes with an urgent call to implement these future techniques as soon as practically possible in order to end the current retardation of advances in global NWP as a result of inadequate satellite sounding data.

2. INTRODUCTION

Unfortunately, there has been little improvement in satellite temperature sounding accuracy as a result of radiometry and/or data processing techniques since the First Global GARP Experiment (FGGE) of 1979. However, during this past decade, greatly improved accuracy of global Numerical Weather Prediction (NWP) has resulted from advances in model resolution, physics, and numerical techniques. Whereas in 1979, the resolution and accuracy of the satellite temperature sounding data generally exceeded that of the forecast generated by NWP; in 1989, the opposite is generally true. As a consequence, we now face the prospect of retarded growth in global NWP until the resolution and accuracy of the global satellite data once again exceed the forecasting skill of the model. Since there are no short-term plans to improve the vertical resolution of satellite sounding

instrumentation, I believe we are now faced with a "crisis" in NWP - a development "drought" which could last throughout the next decade.

Water vapor sounding is a possible exception to the current trend of forecast skill exceeding satellite sounding accuracy. Although current sounding radiometers only provide three channels of water vapor radiance data, it is generally agreed that the current operationally produced water vapor soundings do not represent the full information content of the radiance data; retrieval technique improvements are needed to improve the water vapor sounding accuracy. Furthermore, the Advanced Microwave Sounding Unit (AMSU) to fly on the next series of polar orbiting satellites will provide for the first time several cloud penetrating water vapor profiling channels, thereby leading to even greater improvements in satellite humidity sounding accuracy. On the modelling side, forecasting the humidity distribution accurately is complicated by the small vertical and horizontal scale of water vapor and its sensitivity to local sources of atmospheric buoyancy. Thus, it is unlikely that the accuracy of global NWP humidity forecasts will exceed the observation accuracy possible from satellites, at least in the near term.

In light of the above remarks, this paper deals with the improvement of the sounding retrieval algorithm to provide more accurate humidity profiles. The improvements of future sounding instrumentation required to greatly improve the vertical resolution and accuracy of both temperature and humidity profiles is also emphasized. Both improved sounding instrumentation and retrieval algorithms are needed to improve global NWP.

3. RETRIEVAL TECHNIQUE DEVELOPMENT

3.1 Mathematical Formulation

One of the numerical problems associated with deriving temperature and humidity profiles from satellite observed radiances is caused by the nonlinear interaction of the water vapor emission with the emission from the uniformly mixed gases (CO_2, N_2O, O_2) used to estimate the temperature profile. Because of these spectrally overlapping radiance contributions, the nonlinear equation of radiative transfer has been solved by iteration (Smith, 1968, 1970; Chahine, 1970; Susskind 1982). Unfortunately, because of the nonlinearity of the problem, the solutions exhibit significant

dependence on the "guess" profiles used to initialize the retrieval process.

Recently, a simple method of linearizing the radiative transfer equation (RTE) has permitted the temperature and water vapor components to be separated, permitting a solution without iteration. This advance both increases the efficiency of the sounding retrieval process and at the same time minimizes the solution dependence upon the initial guess profiles.

The linearized form of the RTE results from imposing the monochromatic principal; the total transmittance at a particular wavenumber can be expressed as a product of the transmittances for all the individual gases which are optically active at that wavenumber. Following the derivation described previously by the author (Smith et al., 1987, 1988), one can write a perturbation form of the RTE for N absorbing constituents (e.g., water vapor and the uniformly mixed gases) as

$$\delta R_\nu = W^*_\nu(P_s)\ \delta T_s - \int_o^{P_s} \delta T(P) W^o_\nu(P) dp$$

$$+ \sum_{k=1}^{N} \int_o^{P_s} \delta U^*_k(P)\ W^o_{\nu_k}(p) dp \qquad (1)$$

δR_ν is the deviation of the observed radiance from that computed from initial guess profiles of temperature (T^o) and absorbing gas path length profiles (U^k_i), $\delta T(p)$ is the deviation of the profile of true temperature from the initial profile and $\delta U^*_k(p)$ is the deviation of the absorbing gas path length from that for the initial condition scaled by the temperature lapse rate.

$$\delta U^*_k(p) = \frac{dT(p)}{dp}\ \delta U_k(p)$$

where T is true temperature and δU_k is the departure of the true path length profile for the kth absorbing constituent from the initially assumed profile.

$$W_\nu^*(p_s) = \tau_\nu^o(p_s) \left(\frac{\partial B_\nu}{\partial T}\right)_{T=T_s^o}$$

$$W_\nu^o(p) = \frac{d\tau_\nu^o(p)}{dp} \left(\frac{\partial B_\nu}{\partial T}\right)_{T=T^o(p)}$$

$$W_{\nu k}^o(p) = \frac{d\tau_\nu^o(p)}{dU_k^o(p)} \left(\frac{\partial B_\nu}{\partial T}\right)_{T=T^o(p)} = \tau_\nu^o(p) \frac{d \ln \tau_{\nu k}^o}{dU_k^o(p)} \left(\frac{\partial B_\nu}{\partial T}\right)_{T=T^o(p)}$$

where $\tau_\nu^o(p)$ is the total transmittance of the atmosphere above pressure level for the initial temperature and water vapor condition, whereas $\tau_{\nu k}(p)$ is the transmittance for an individual constituent (e.g., water vapor or CO_2).

If we assume that there is no error in the initial concentration profiles for the uniformly mixed gases, then we can write

$$\delta R_\nu = W_\nu^*(p_s)\delta T_s - \int_o^{p_s} \delta T(p) W_d(p) dp - \int_o^{p_s} \delta T_w(p) W_w(p) dp \qquad (2)$$

with

$$W_d(p) = \tau_\nu^o(p) \frac{d\ln\tau_{\nu_d}^o(p)}{dp} \left(\frac{\partial B}{\partial T}\right)_{T=T^o(p)}$$

$$W_w(p) = \tau_\nu^o(p) \frac{d\ln\tau_{\nu_w}^o(p)}{dp} \left(\frac{\partial B}{\partial T}\right)_{T=T^o(p)}$$

$$\delta T_w(p) = \delta T(p) - \delta U_w(p) \left[\frac{dT(p)}{dU_w^o(p)}\right] \qquad (3)$$

where the subscript w refers to water vapor and the subscript d refers to all the remaining uniformly mixed "dry" gases.

Equation (2) is a completely linear form of the RTE from which a direct matrix inverse solution for $\delta T(p)$ and $\delta T_w(p)$ can be achieved. From $\delta T(p)$ and $\delta T_w(p)$, Equation (3) can be used to determine the precipitable water vapor profile:

$$U_w(p) = U_w^o(p) + (\delta T(p) - \delta T_w(p)) \bullet \frac{dU^o{}_w(p)}{dT(p)} \tag{4}$$

where

$$T(p) = T^o(p) + \delta T(p)$$

The linear matrix inverse solution of (2) is given by

$$t = (A^T A + \gamma \epsilon I)^{-1} A^T r \tag{5}$$

where t is a vector composed of δT_s, δT, and δT_w for all the numerical quadrature levels (i.e., the length of the t vector is twice the number of pressure levels plus one), A is a matrix whose elements are the W_s^*, W_d, and W_w for each observation frequency and pressure level, and r is a vector of the δR_ν's. The superscript T denotes matrix transposition, I is the identity matrix, and γ is a Lagrangian multiplier used to stabilize the near singular matrix, $A^T A$, prior to inversion. The elements of the vector ϵ are the expected errors of measurement.

3.2 Applications to TOVS

The completely linearized solution has been implemented in the International TOVS Processing Package (ITPP-3) and applied to TOVS radiances. The results are compared to the original ITPP-3 simultaneous (Smith et al., 1985), but nonlinear, solutions achieved from the same data. The case is the March 9, 1982 ALPEX data set used by the International TOVS (ITOVS) Working Group for testing algorithm improvements The first guess used for the solutions was "climatology." Figure 1 shows RMS differences with radiosondes. As can be seen, both lower tropospheric temperature and middle and upper tropospheric dewpoint accuracy is improved with the ITPP-3 algorithm using solutions of the linearized RTE.

Figure 2 shows analyses of the two consecutive orbits of TOVS derived dewpoint temperature at 400 and 700 mb using solutions of the linearized

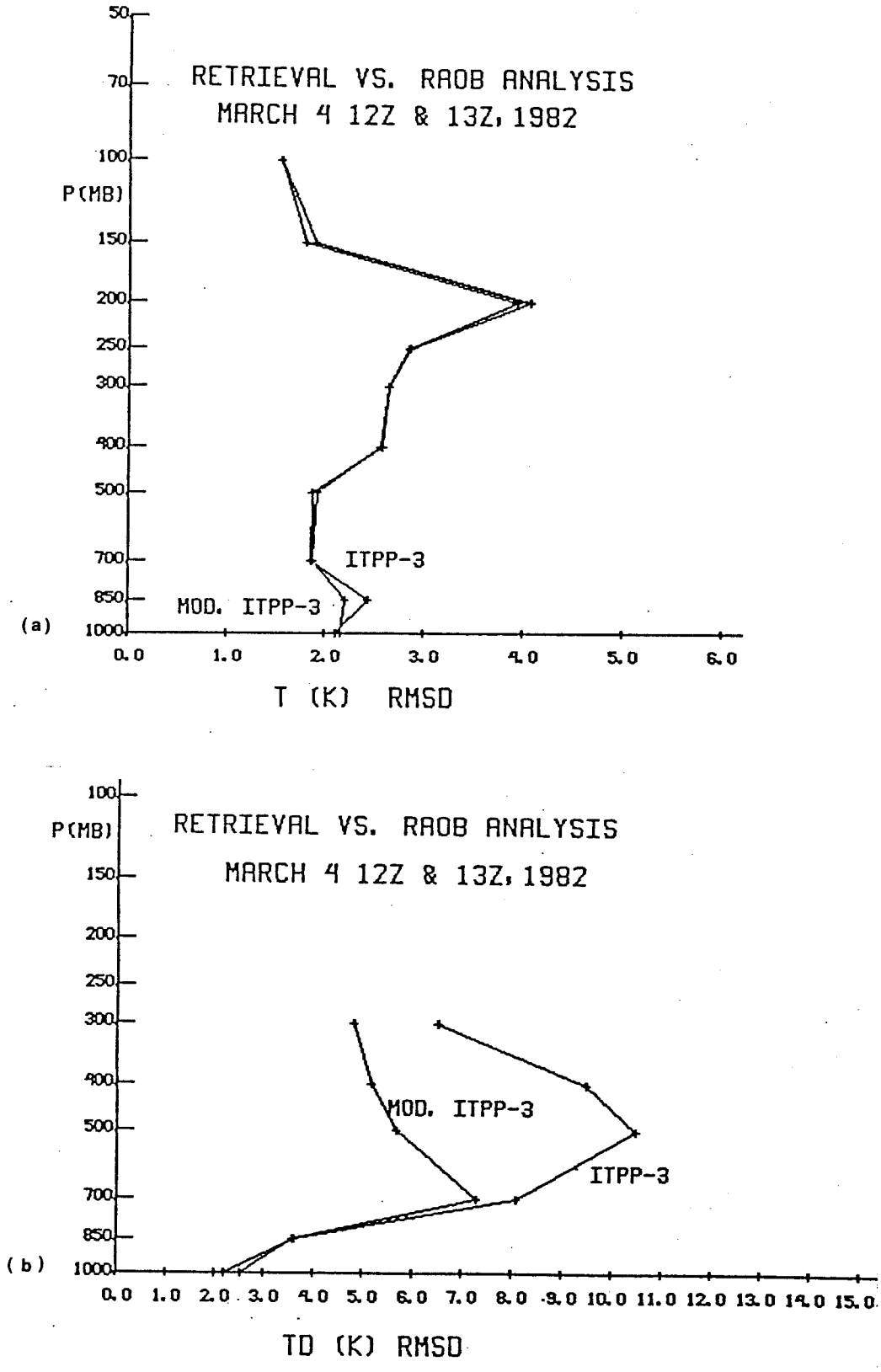

Fig. 1. Root mean square differences between TOVS retrievals and an analysis of radiosonde data: (a) temperature derived using the original ITPP-3 (non-linear), and using the modified ITPP-3 (linear) method, and (b) dewpoint.

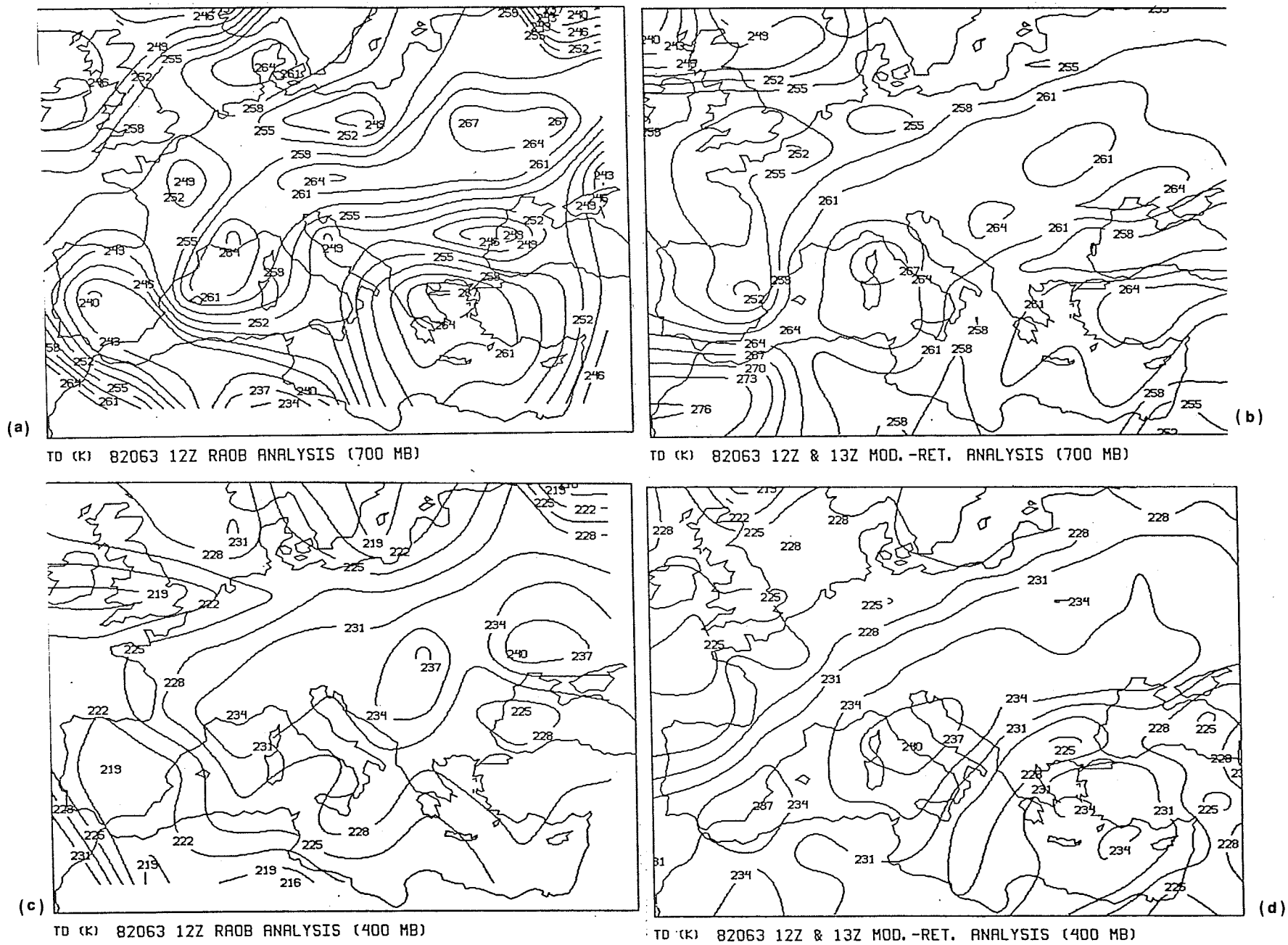

Fig. 2. Analyses of radiosonde dewpoint observations for 700 mb (a) and 400 mb (c), and TOVS retrieved dewpoints for 700 mb (b) and 400 mb (d) over Europe for the ALPEX day, 4 March 1982.

RTE. Analyses of radiosonde data are provided to verify the TOVS values retrieved through the solution of the linearized RTE. It can be seen that there is good general agreement between the analyses of TOVS dewpoints and the analyses of radiosondes. However, the satellite data fails to capture the extremes as observed by the point measuring radiosonde. The conservatism of the satellite retrieved moisture field is due entirely to the limited number of moisture channels and their very poor vertical resolution as discussed in the next section.

4. IMPROVED SOUNDING INSTRUMENTATION

4.1 Background

Because of the temperature and water vapor profiling capabilities needed to support global NWP, sounding radiometers with greatly improved vertical resolution are urgently needed. To obtain the vertical temperature and moisture profile resolution required, theoretical studies show that the sounding instrument must achieve near continuous spectral coverage throughout the 600-2600 cm^{-1} region with a spectral resolution ($\lambda/\Delta\lambda$) of order 1000 (Smith et al., 1979, 1983; Fleming, 1987). The high spectral resolution is needed to avoid smearing the upwelling radiance contributions from relatively opaque absorption lines with the contributions from the relatively transparent regions in between the absorption lines. For example, in the thermal emission bands of CO_2, a spectral resolution of 0.7 cm^{-1} is needed in the 600-800 cm^{-1} (15 μm) region and 2 cm^{-1} in the 2300-2400 cm^{-1} (4.3 μm) region. Although the required spectral coverage and spectral resolution is beyond the capabilities of filter wheel radiometers now flown on satellites, it can be achieved using an interferometer.

A High resolution Interferometer Sounder (HIS) instrument has been developed and flown aboard the NASA U2 and ER2 aircraft to prove the sounding performance capabilities of an interferometer (Revercomb et al., 1987, 1988a, 1988b). Ground calibration tests and airborne science missions have demonstrated the ability of the HIS to measure radiometrically accurate emission spectra with a resolution far exceeding the performance of contemporary filter radiometers. Radiance spectra have been obtained during more than 40 aircraft missions with a resolution of 0.35 cm^{-1} in the 600 to 1100 cm^{-1} region and 0.7 cm^{-1} in the 1100-2700 cm^{-1} region, as compared to the typical 15.0-60.0 cm^{-1} resolution of filter radiometers, such as the HIRS flown on the NOAA satellites.

Figure 3 shows a typical spectrum of infrared radiation brightness temperature sensed by the HIS. The bandwidths of the filters of the HIRS sounding radiometer are superimposed. As can be seen, the filter wheel radiometer severely smears the fine scale spectral radiance structure of the atmosphere. The spectral smearing causes unwanted absorption contamination in atmospheric "windows" used for sensing the earth's surface temperature, and it greatly limits the vertical resolution of temperature and water vapor profiles because it broadens the atmospheric weighting functions (Fig. 4).

In Fig. 5, the vertical resolution of atmospheric temperature and water vapor profiles as sensed by the HIRS filter wheel radiometer is compared to that of a satellite-borne HIS interferometer. These vertical resolution functions were determined using the definition given by Rodgers (1987). Analytically, the retrieved atmospheric temperature profiles (dry or water vapor) are related to the true atmospheric profiles through the relation

$$T_{RTVL}(p') = \int_{o}^{p_s} T(p)\phi(p',p)\, dp$$

where p' is the pressure of the retrieved temperature, T_{RTVL}, p_s is surface pressure, $T(p)$ is the true atmospheric temperature profile, and $\phi(p',p)$ is the vertical resolution function. The function $\phi(p',p)$ depends upon: (1) the weighting function sharpness (i.e., spectral resolution), (2) the number of spectral channels, and (3) the measurement noise. The large number of spectral channels produced by an interferometer serves to both increase the number of spectrally independent pieces of information about the profiles as well as to reduce the system noise through the statistical averaging of vertically redundant observations performed by the inversion process.

As can be seen in Fig. 5, a factor of 2-3 improvement in the vertical resolution of atmospheric temperature and water vapor results from the much higher spectral resolution and continuous spectral coverage provided by the interferometer.

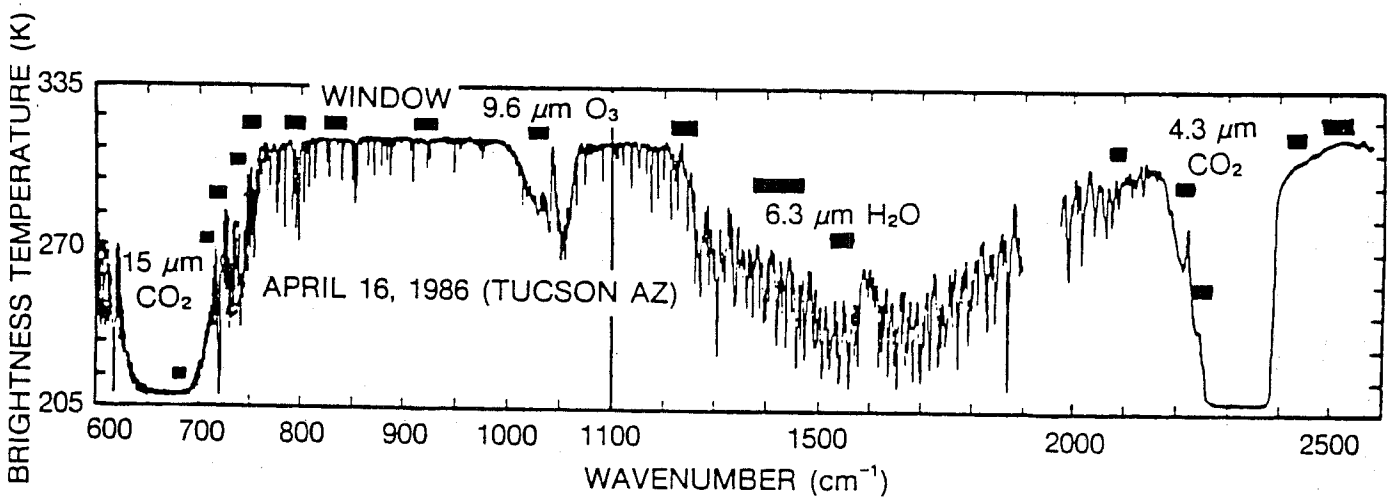

Fig. 3. A spectrum of upwelling radiance observed with the HIS interferometer from the 55 mb pressure altitude of the NASA U2 aircraft. Superimposed are bars indicating the spectral positions and bandwidths of the HIRS radiometer.

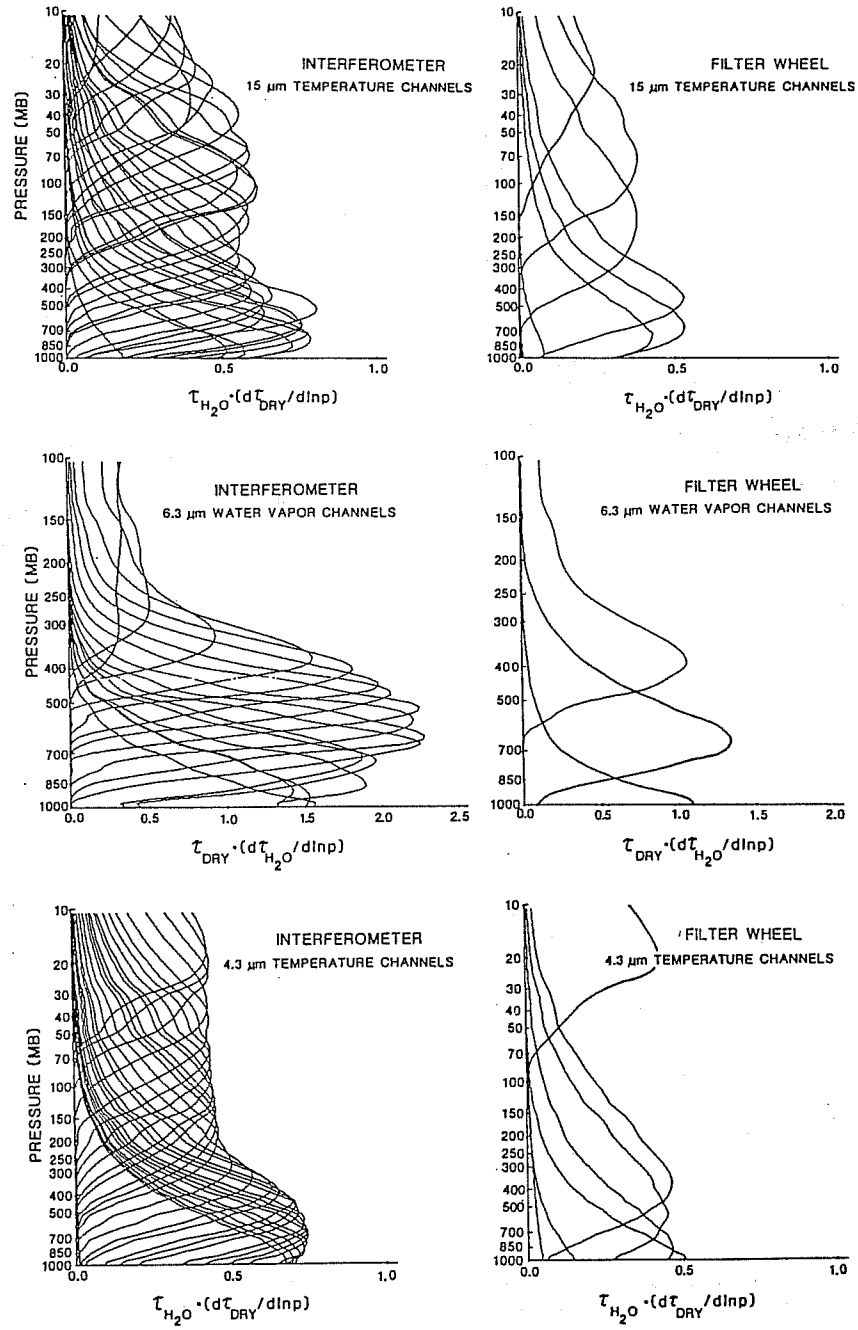

Fig. 4. Temperature and water vapor component weighting functions for a small selection HIS "interferometer" spectral channnels and for the HIRS "filter wheel" sounding channels. Note factor of 2 the abcissa scale change between the temperature and water vapor diagrams.

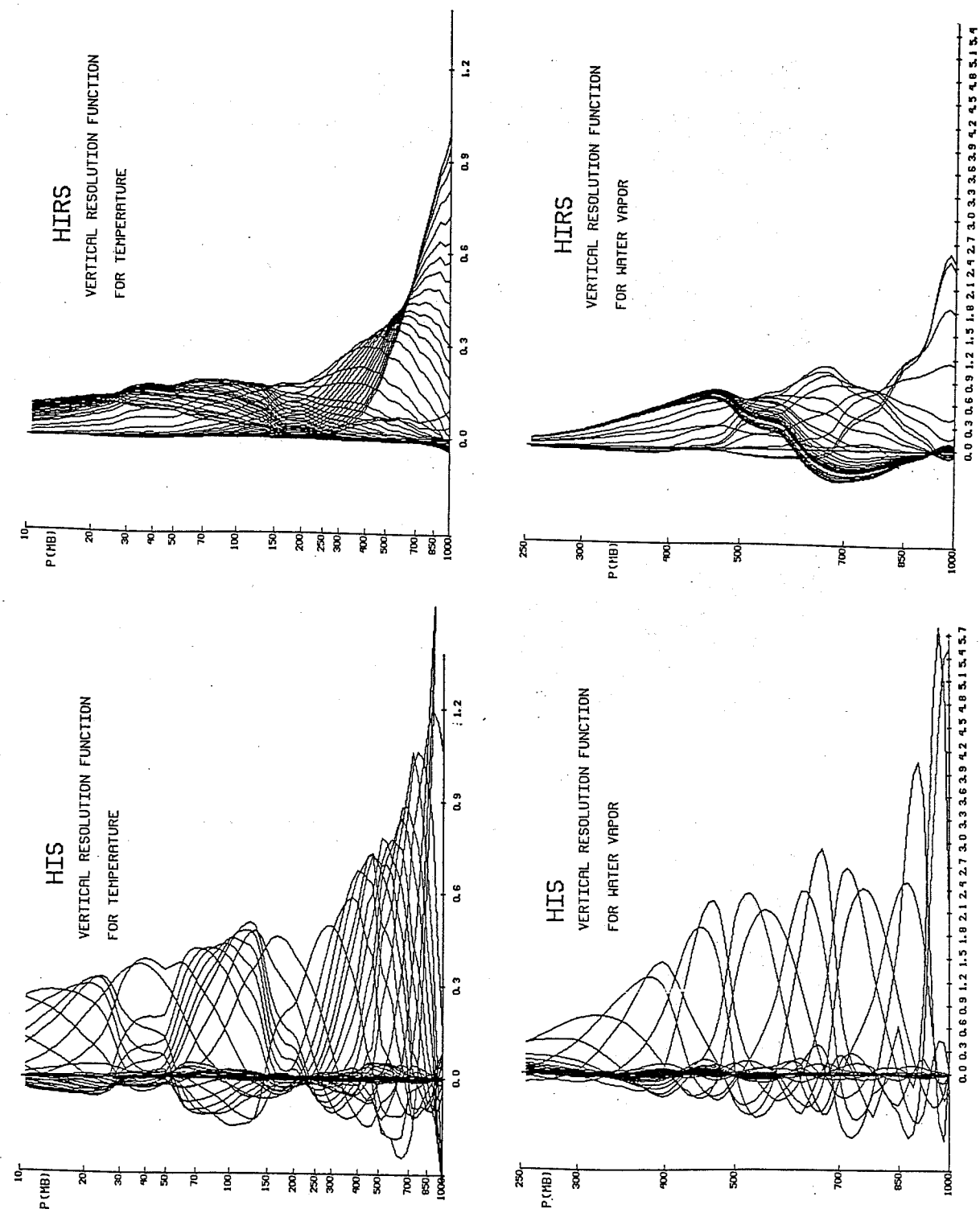

Fig. 5. Vertical resolution functions for ambient temperature and water vapor temperature profiles associated with the HIS interferometer and HIRS filter radiometer. Note the factor of 4 abcissa scale change between the temperature and water vapor diagrams.

Figures 6 and 7 are provided to separate the impacts of higher spectral resolution and the much smaller system noise gained through quasi-continuous spectral sampling. Shown in Fig. 6 are example vertical resolution functions associated with an interferometer with a spectral resolution of the HIS and the nominal noise equivalent temperature of 0.25°K, for a 260°K scene temperature (D). Also shown is the vertical resolutions associated with a lower spectral resolution interferometer with the nominal measurement noise condition (B) and the vertical resolution of the HIRS (A) as a reference with respect to compare the improved performance achieved through continuous spectral coverage, higher spectral resolution, and reduced measurement noise. Curve C represents an interferometer with one-tenth spectral resolution, but with only $1/\sqrt{10}$ the nominal noise equivalent temperature, 0.08°K for a 260°K scene temperature. As can be seen, the higher spectral resolution but higher noise measurements provide significantly higher vertical resolution than the lower spectral resolution, but lower noise, interferometer measurement. Figure 7 shows the vertical resolution as expressed in the Guassian half-width of the $\phi(p',p)$ functions for the four measurement situations and Fig. 8 shows the RMS retrieval errors associated with the four measurement conditions using the error analysis method described by Smith et al. (1989). In final analysis, Figs. 5, 6, 7, and 8 all indicate that major improvements in vertical sounding resolution are achieved by obtaining quasi-continuous spectral sampling, which greatly reduces system noise (by the square root of the number of spectrally independent observations), and by increasing the spectral resolution ($\lambda/\Delta\lambda$) to 1000/1 or better, thereby increasing the vertical independence of the spectral radiance observations.

4.2 HIS Profile Retrieval Methodology

For the retrieval of atmospheric profiles from the HIS, it is desirable to utilize all the spectral observations in a simultaneous solution for temperature, water vapor and other desired absorbing constituents (e.g., ozone, methane, etc.). The general solution of the perturbation form of the RTE given by Equation (2) is the "physical simultaneous" least squares retrieval algorithm (Smith et al., 1988).

$$t = DA_o^T t_b = Dt^* \qquad (6)$$

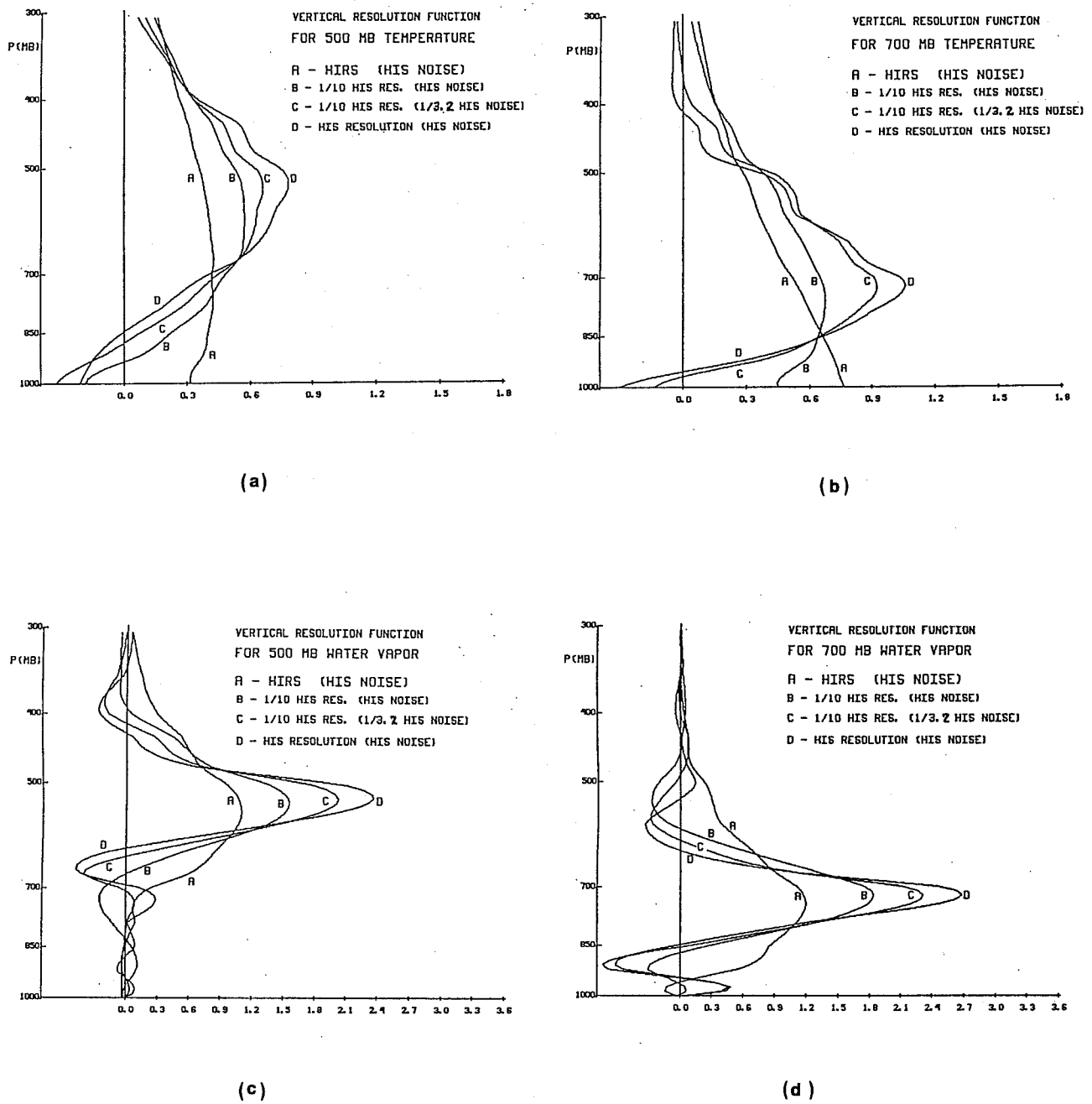

Fig. 6. Vertical resolution functions for 500 mb temperature (a), 700 mb temperature (b), 500 mb water vapor temperature (c), and 700 mb water vapor temperature (d). Four different plots are shown: (A) HIRS spectral with a NEΔT of 0.25°C, (B) low spectral resolution (1/10 HIS) spectra with a NEΔT of 0.25°C, (C) low resoluton spectra with a NEΔT of 0.08°C, and (D) HIS spectral resolution with a NEΔT of 0.25°C.

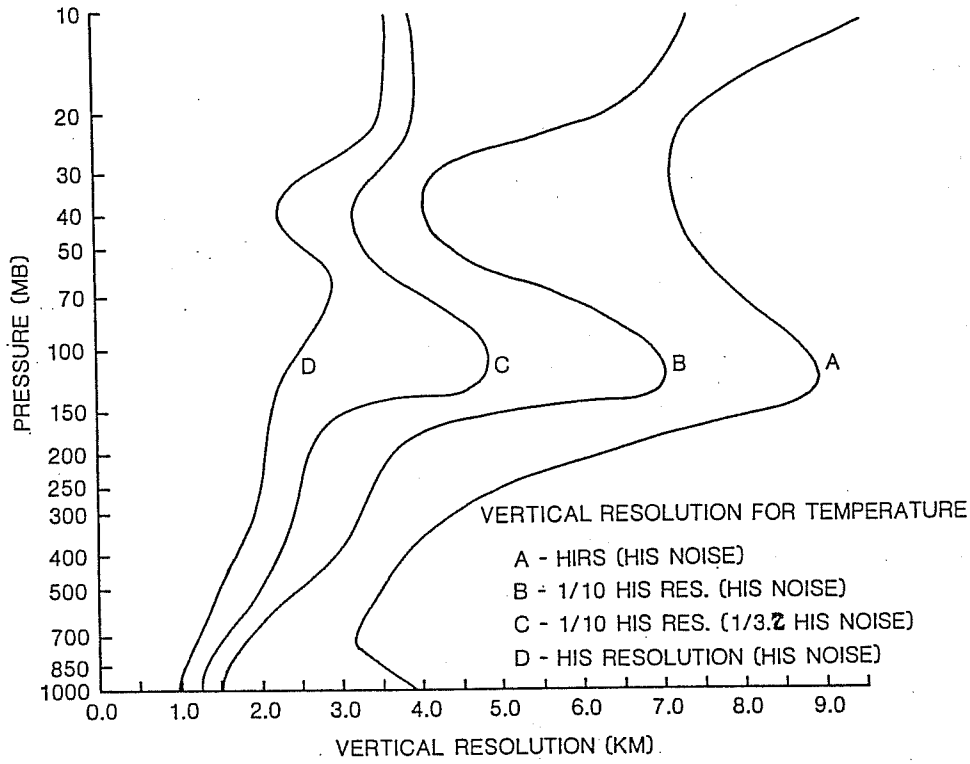

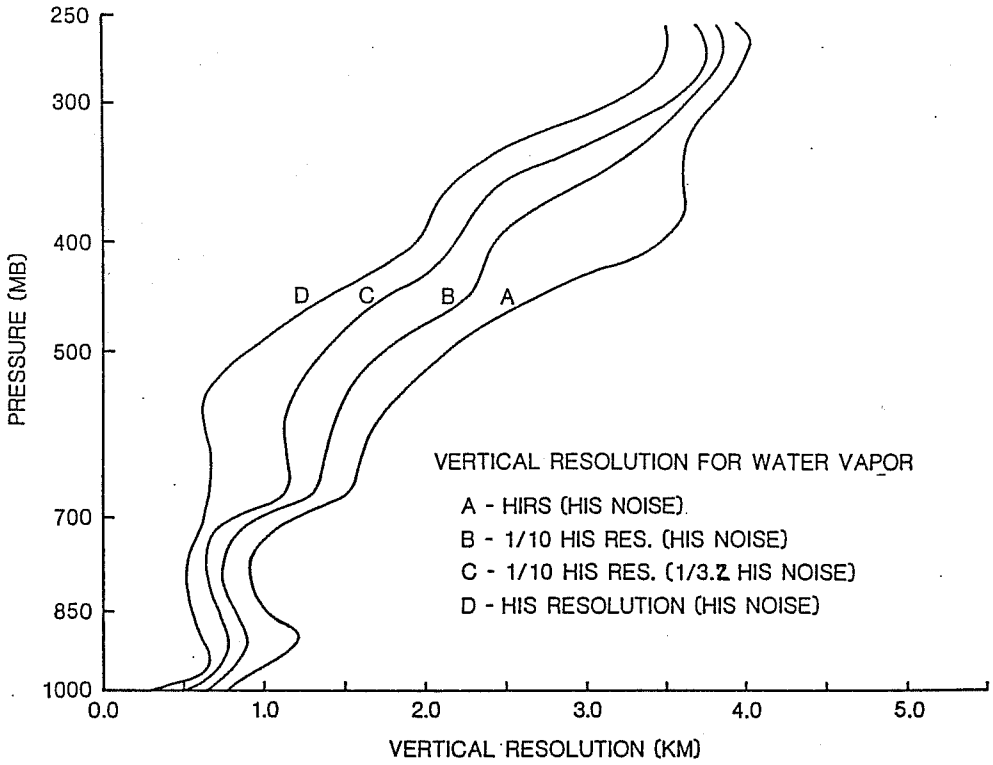

Fig. 7. Gaussian half-width of vertical resolution functions as a function of altitude for each of the four measurement situations shown in Figs. 6 and 7.

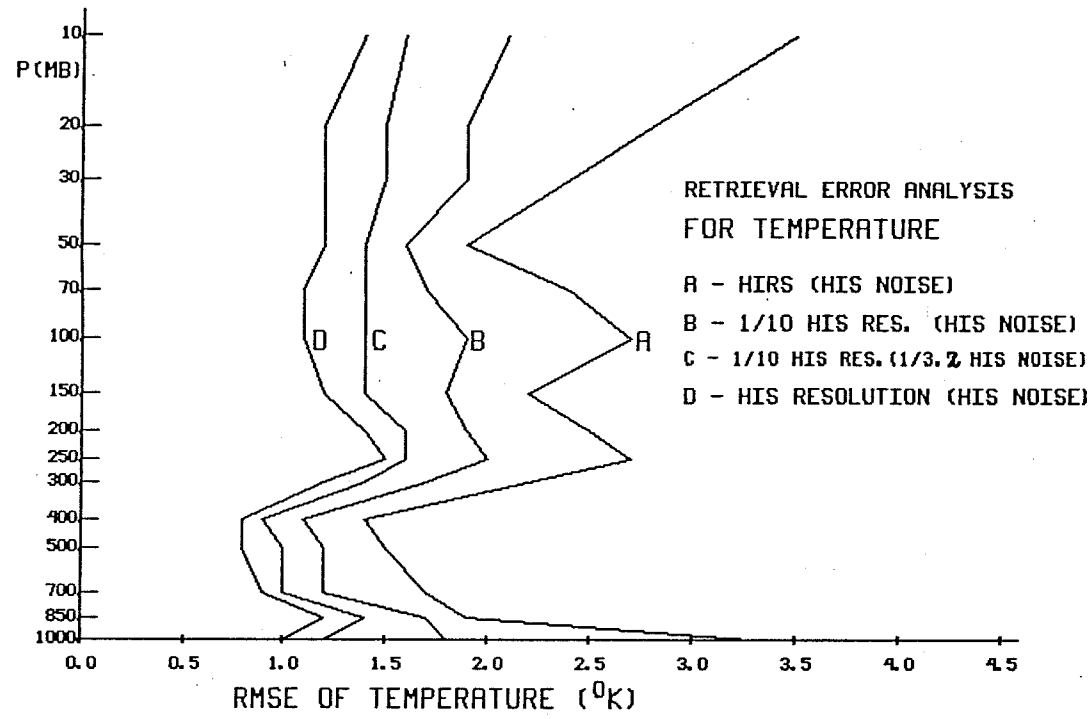

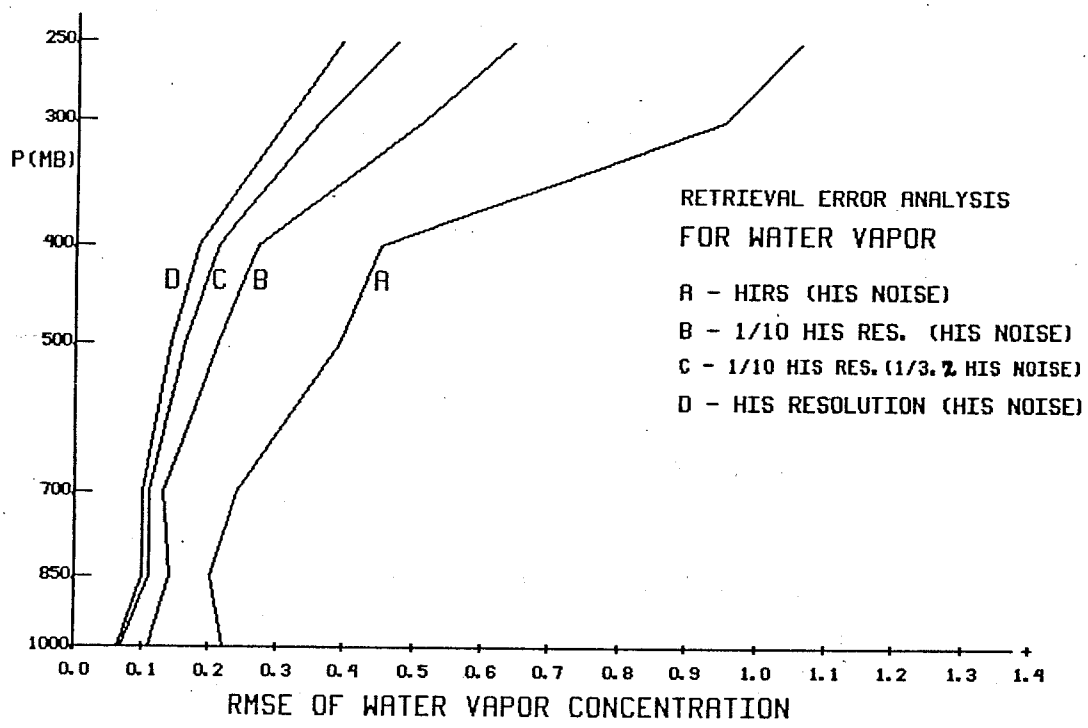

Fig. 8. Temperature (°K) and vertically integrated water vapor concentration profile (%/100) retrieval errors for each of the four measurement situations shown in Figs. 6 and 7.

where t is a vector of the deviations of the desired atmospheric variables from an ensemble mean condition, t_b is a vector of observed brightness temperature deviations from the mean condition, A_o^T is the transpose of the profile weighting function matrix, partitioned into "dry" and "wet" components as required for the simultaneous solution, and D is a "deconvolution" matrix. In its application, we define

$$t^* \equiv A_o^T \, (t_b + \beta) \tag{7}$$

where β is the systematic error in calculated brightness temperature due to uncertainties in the spectroscopy and errors in the numerical methods used to define the atmospheric transmittance spectra. The elements of A_o are

$$a_{ij} = W_{ij} \; / \sum_{i=1}^{M} W_{ij}$$

with

$$W_{ij} = f_{ij} \; \tau(\nu_i, p_j) \; d \ln \tau_k \; (\nu_i, p_j) \; / \; \sigma_{\epsilon(\nu_i)},$$

$$f_{ij} = \partial B \; (\nu_i, \; T_j^o)/\partial T,$$

B is Planck radiance, and T is temperature. The zero superscript refers to the mean temperature profile condition. The subscripts i,j,k denote spectral wavenumber, atmospheric pressure level, and atmospheric absorbing constituent, respectively. The transmittance of the atmosphere between the instrument and pressure level, p_j, is $\tau(\nu_i, p_j)$ whereas that due to an individual absorbing constituent (e.g., water vapor) is $\tau_k(\nu_i, \; p_j)$. The derivative is respect to the vertical coordinate. Here we treat the spectrum as composed of uniformly mixed constituents (k=1) and water vapor (k=2). Consequently, the first half of the vector t is the dry atmospheric temperature profile as sensed by the uniformly mixed gas portion of the absorption/emission spectrum whereas the second half of t is the temperature profile as sensed by the water vapor portion of the absorption/emission spectrum. It is noted that if the actual water vapor profile is equal to the mean profile, then the two temperature profiles, wet and dry, are identical. For all other conditions, the actual moisture profile is a function of the discrepancy between the wet and dry

temperature components. Consequently, the mixing ratio profile can be approximated from a linear combination of dry and wet component temperature profiles. The quantity $\sigma_{\epsilon(\nu i)}$, the standard deviation of the radiance due to measurement noise and the noise in theoretical radiative transfer computations, is included to weight those spectral regions which have the lowest noise most heavily in the profile solutions.

The vector t^*, as defined by (7), can be thought of as the vertically smoothed temperature profile depicted by the convolution of the spectral weighting functions with the radiant brightness temperatures. Numerically,

$$t^*(p_j) = \sum_{i=1}^{M} W_{ij}(t_{bi}+\beta_i) \tag{8}$$

that is, the convoluted temperature profile deviation from the mean is given by the spectrally weighted average brightness temperature spectrum deviation from the mean spectrum. This form for t^* is identical to the generalized iterative retrieval solution used for processing grating spectrometer and filter wheel radiometer data. However, because of the large number of spectral radiance observations (~4000) with the HIS, iteration of (3) is prohibitive due to the very large amount of radiative transfer computation involved to update W_{ij} and the mean brightness temperature spectrum with the spectrum computed from a prior retrieval. Instead, t^* serves here as the smooth first approximation of the true profile whose enhanced vertical structure is retrieved through the application of the deconvolution matrix, D. The D matrix is determined by the least squares matrix inversion solution

$$D = (TT^{*T})\ (T^*T^{*T})^{-1} \tag{9}$$

where T is a matrix of dry bulb temperature and water vapor mixing ratio profile deviations from their mean for a statistical ensemble of soundings and T^* is a matrix of the smoothed temperature (dry and wet component) profiles from their ensemble mean values. T^* is specified by radiative transfer computation of W_{ij} and t_{bi}. Random errors of measurement are simulated using a random number generator and added to t_{bi} in order to stabilize the solution against actual instrument noise. For the generation of T^* used in (9), β is assumed to be equal to zero since here T^* is based

solely on radiative transfer theory. However, when D is applied to real spectral brightness temperature observations, β must be applied to t_b (Eq. 8) in order to account for systematic errors in the radiative transfer model.

During the COmbined Huntsville Meteorological EXperiment (COHMEX), the HIS flew aboard the NASA U2/ER2 aircraft. A few example results achieved during COHMEX are presented below to illustrate the sounding capabilities of the HIS.

4.3. Experimental Results

Figure 9 shows two example comparisons of radiosondes with retrievals of temperature and dewpoint profiles from actual HIS spectral radiances observed on June 19, 1986. (It is noted that the "D" matrix and initial mean profile used for these retrievals is achieved from a statistical ensemble of radiosonde profiles observed during the COHMEX. We can see from these comparisons that the agreement of the radiance derived profiles with the radiosonde is close to the theoretical expectation (Fig. 8). The fine scale water vapor structure retrieved is particularly noteworthy.

Figure 10 is presented to show the improvement in vertical resolution and accuracy of HIS profile retrievals over those achieved with current satellite filter radiometer sounders. In this case, the filter wheel sounder is the VISSR Atmospheric Sounder (VAS) aboard the GOES satellite. NOAA TOVS soundings have a vertical resolution similar to that achieved with the VAS. As can be seen, whereas VAS depicts the broad scale profiles of temperature and moisture, HIS is capable of resolving finer scale vertical structure features. Once again, the most noticeable improvement appears in the moisture profile retrieval. In order to illustrate the water vapor sensing capability of the HIS, Figs. 11 and 12 show vertical cross-sections along the flight tracks of the NASA U2 and ER2 on June 15 and June 19, 1989, respectively. Both flight tracks are over northern Alabama and Tennessee, but as can be seen from the HIS data, the meteorological characteristics are quite different for the two observation days. On June 15, the HIS cross-section reveals an intense boundary layer whose top was near the 850 mb level. Indeed, cloud observations revealed that the top of a low level scattered cumulus deck was near the 850 mb level. The rapid drying and stabilizing temperature structure just above

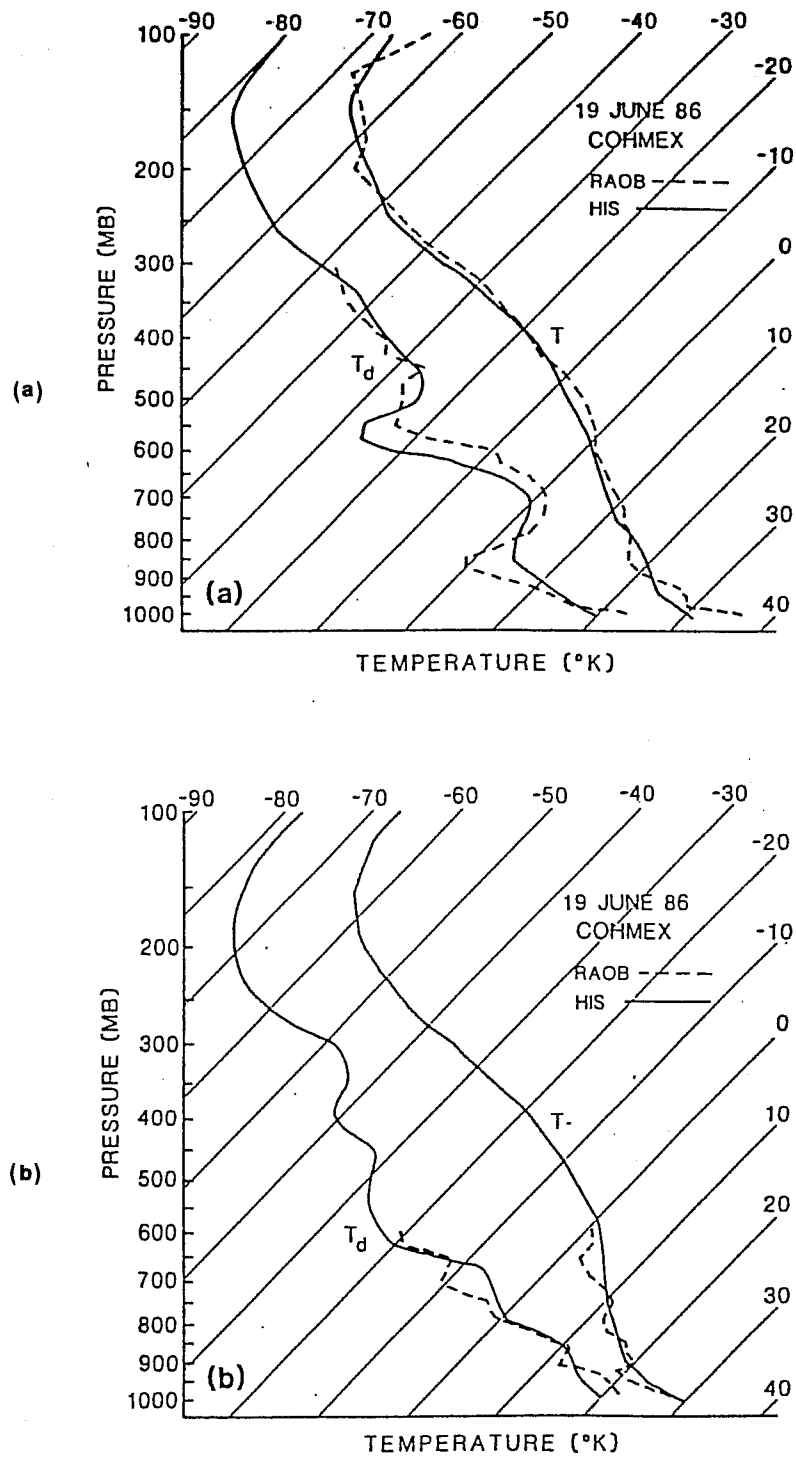

Fig. 9. Examples of two COHMEX radiosondes, (a) and (b) above, compared to retrievals of temperature and dewpoint from actual HIS spectral radiances observed June 19, 1986.

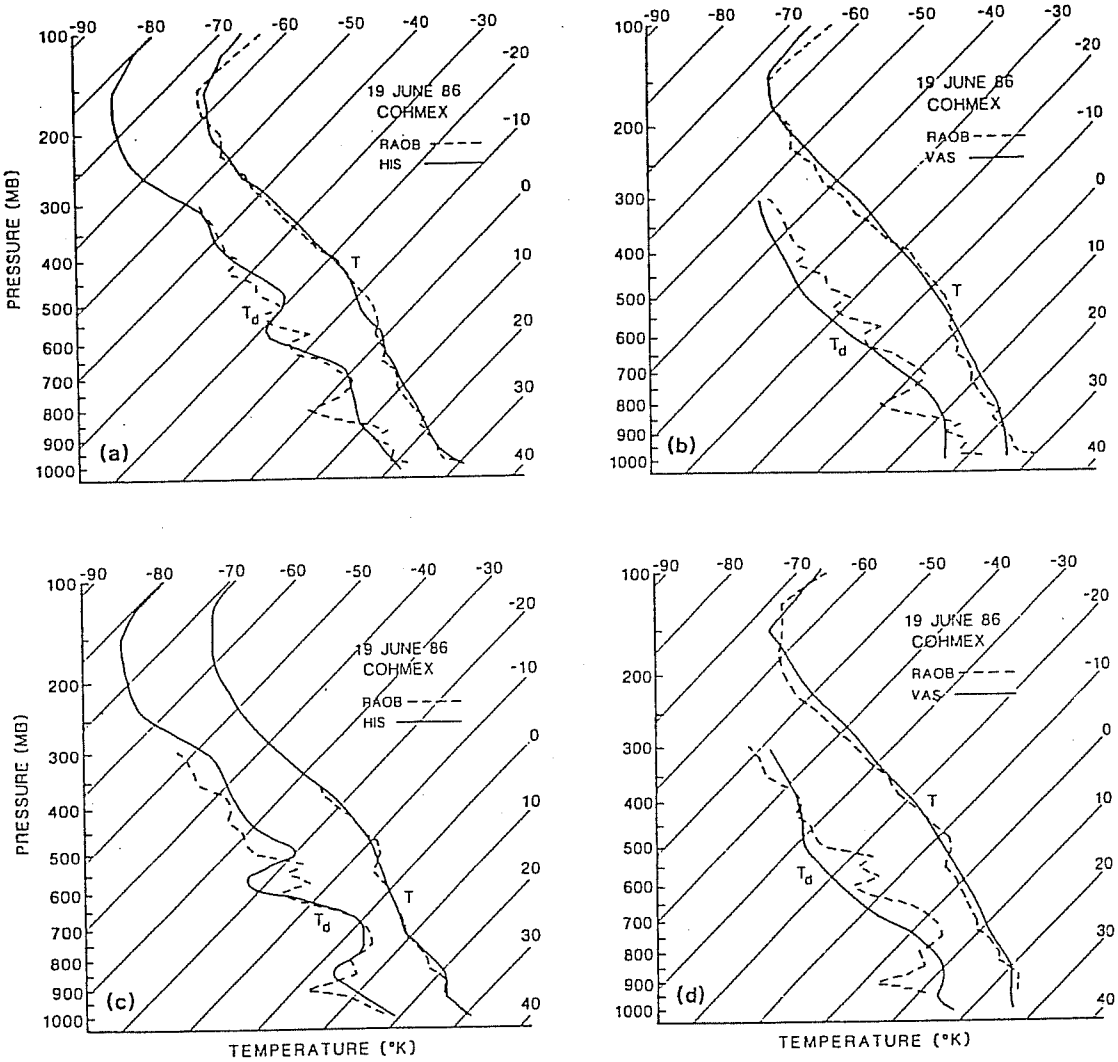

Fig. 10. The improvement in vertical resolution of the HIS (a) is apparent when compared to a coincident satellite retrieval using the VAS filter wheel sounder (b). In another example from COHMEX, a HIS retrieval (c) is compared to a coincident VAS retrieval (d).

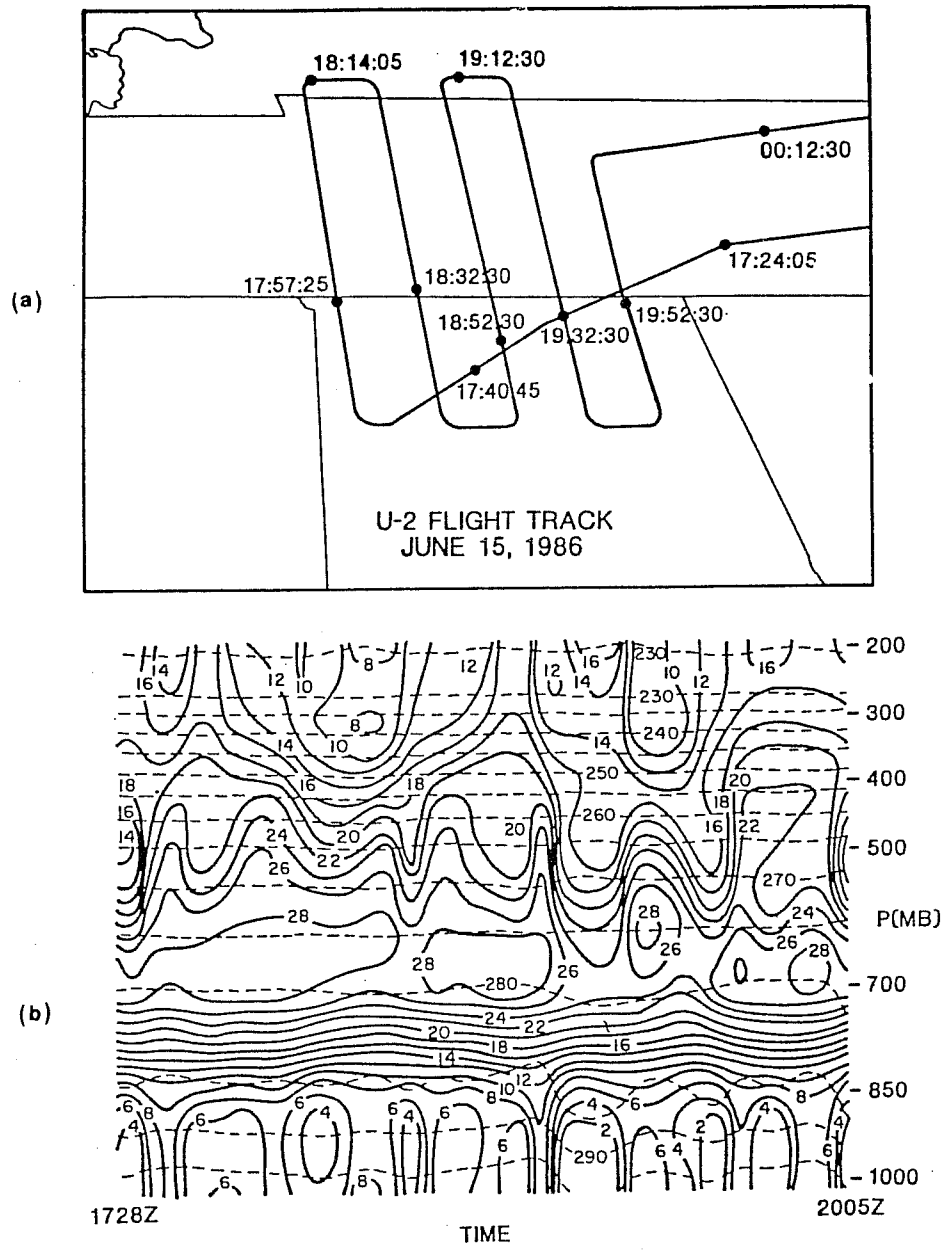

Fig. 11. (a) Flight track of the NASA/U2 over northern Alabama and Tennessee on 15 June 1986. The times of various aircraft are denoted in hours, minutes, and seconds of central daylight time. (b) Vertical/tie cross-section of atmospheric temperature (dashed) and dewpoint depression (solid) beneath the U2 flight track as retrieved from HIS spectra.

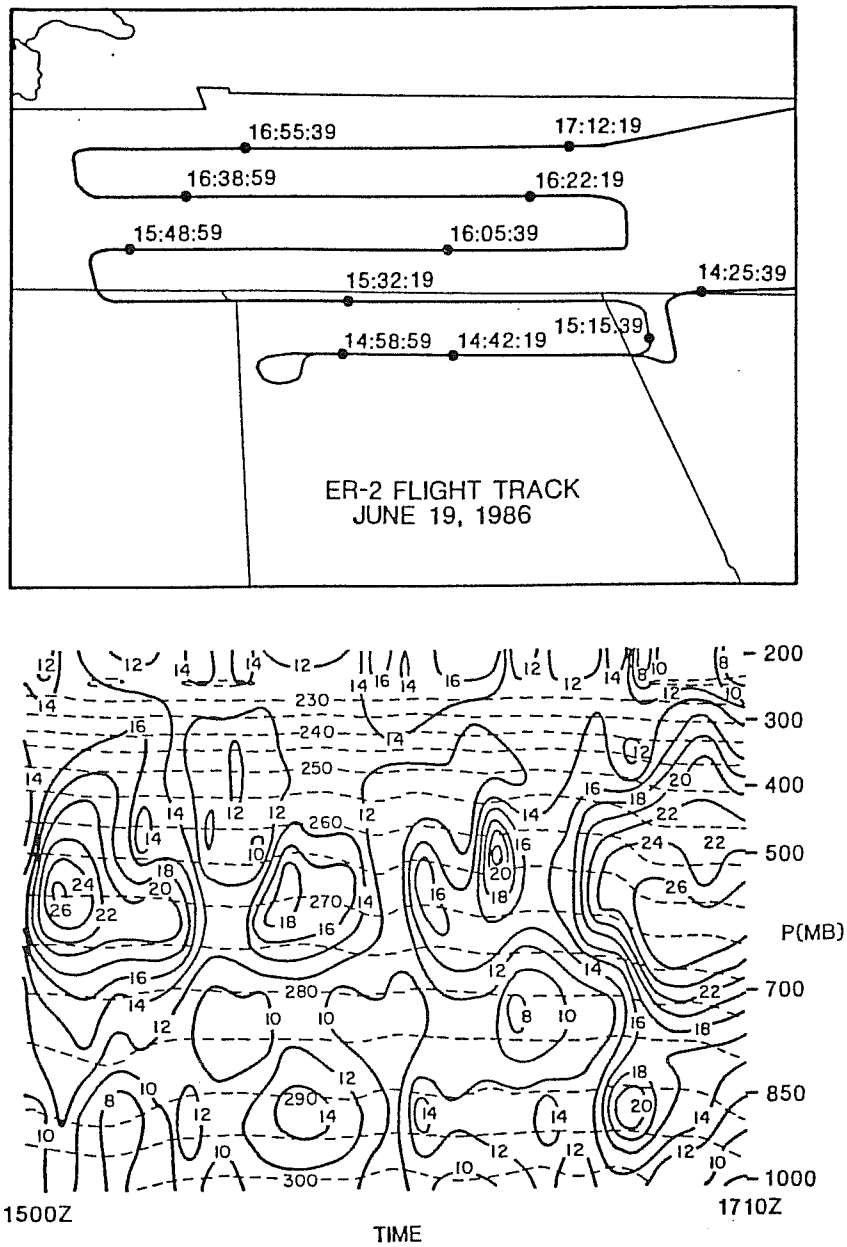

Fig. 12. Same as Fig. 11, but for 19 June 1986.

the boundary layer (850-700 mb) is clearly evident in the HIS cross-section analysis. Also, the largest horizontal variability in moisture occurs within the 200-400 mb layer where the aircraft traverses a moisture front located across central Tennessee. On June 19, the meteorological condition is quite different. The HIS cross-section does not reveal the existence of an intense boundary layer and this was supported by the fact that no boundary layer cumulus clouds or haze was observed. Contrary to the June 15 observation, the largest horizontal variability of atmospheric moisture occurs lower in the atmosphere within the 400-700 mb layer. In both cases, the vertical resolution of the retrieved water vapor structure is striking. In this regard, the HIS sounding capabilities are unique; that is, no other sensor is capable of providing the vertical and horizontal sounding detail obtained with the airborne HIS.

5. FURTHER REMARKS

Because there has been little improvement in satellite sounding capabilities during the past decade, progress in global NWP models is now limited by the vertical resolution and accuracy of the satellite data. Indeed, we now face an extensive "drought" in the advancement of global forecasting until the satellite instrumentation is improved. Remote sounding research during the past decade indicates that greatly improved performance can be achieved by the replacement of contemporary filter radiometers with high spectral resolution Michelson interferometer spectrometers. (An alternative to the Michelson interferometer is a large detector array grating spectrometer, but this technology is just now under development as part of NASA's Eos program.) Experimental airborne measurements confirm the theoretical expectations of improving the vertical resolution by a factor of two or more, depending upon altitude, and achieving an accuracy near 1°C. Because of the crisis in global NWP due to the vertical resolution limitations of contemporary satellite soundings, the world meteorological community should cooperatively work to implement the currently available high spectral resolution interferometer technology on operational satellites as soon as practically possible.

6. REFERENCES

Chahine, M. T., 1970: A general relaxation method for inverse solution of the full radiative transfer equation. J. Atmos. Sci., 27, 960.

Fleming, H. E., and L. L. Barnes, 1987: Satellite tomographic remote sensing retrieval methods. RSRM 87: Advances in Remote Sensing Retrieval Methods. A. Deepak, H. Fleming, J. Theon (Eds.), A. Deepak Publishing, Hampton, VA.

Revercomb, H. E., H. Buijs, H. B. Howell, R. O. Knuteson, D. D. LaPorte, W. L. Smith, L. A. Sromovsky, and H. W. Woolf, 1987: Radiometric calibration of IR interferometers: experience from the High-resolution Interferometer Sounder (HIS) aircraft instrument. RSRM 87; Advances in Remote Sensing Retrieval Methods. A. Deepak, H. Fleming, J. Theon (Eds.), A. Deepak Publishing, Hampton, VA.

Revercomb, H. E., D. D. LaPorte, W. L. Smith, H. Buijs, D. G. Murcray, F. J. Murcray, and L. A. Sromovsky, 1988a: High-altitude aircraft measurements of upwelling IR radiance: prelude to FTIR from geosynchronous satellite. Microchimica Acta [Wien] II, 439-444.

Revercomb, H. E., H. Buijs, H. B. Howell, D. D. LaPorte, W. L. Smith, and L. A. Sromovsky, 1988b: Radiometric calibration of IR Fourier transform spectrometers: solution to a problem with the High resolution Interferometer Sounder (HIS). Appl. Optics, 27, 3210-3218.

Rodgers, C. D., 1987: A general error analysis for profile retrievals. RSRM 87; Advances in Remote Sensing Retrieval Methods. A. Deepak, H. Fleming, J. Theon (Eds.). A. Deepak Publishing, Hampton, VA.

Smith, W. L., 1968: An improved method for calculating tropospheric temperature and moisture from satellite radiometer measurements. Mon. Wea. Rev., Vol. 96, No. 6, 387-396.

Smith, W. L., 1970: Iterative solution of the radiative transfer equation for temperature and absorbing gas profiles of an atmosphere. Appl. Optics, 9, 1993-1999.

Smith, W. L., H. B. Howell, and H. M. Woolf, 1979: The use of interferometric radiance measurements for sounding the atmosphere. J. Atmos. Sci., 36, 566-575.

Smith, W. L., H. E. Revercomb, H. B. Howell, and H. M. Woolf, 1983: HIS - a satellite instrument to observe temperature and moisture profiles with high vertical resolution. Fifth Conference on Atmospheric Radiation, Baltimore, MD, AMS, October 31-November 4, Boston, MA.

Smith, W. L., H. M. Woolf, C. M. Hayden, and A. J. Schreiner, 1985: The Simultaneous retrieval export package. Technical Proceedings of the Second International TOVS Study Conference, W. P. Menzel (Ed.), 224-253.

Smith, W. L., H. M. Woolf, H. B. Howell, H.-L. Huang, and H. E. Revercomb, 1987: The simultaneous retrieval of atmospheric temperature and water vapor profiles - applications to measurements with the High spectral resolution Interferometer Sounder (HIS). RSRM 87; Advances in Remote

Sensing Retrieval Methods. A. Deepak, H. Fleming, J. Theon (Eds.). A. Deepak Publishing, Hampton, VA.

Smith, W. L., H. M. Woolf, H. B. Howell, H. E. Revercomb, and H.-L. Huang, 1988: High resolution interferometer sounding - the retrieval of atmospheric temperature and water vapor profiles. Third Conference on Satellite Meteorology and Oceanography of the AMS, February 10-5 Anaheim, CA.

Smith, W. L., H. M. Woolf, and H. E. Revercomb, 1989: A linearized form of the radiative transfer equation for the simultaneous retrieval of atmospheric temperature and absorbing constituent profiles. To be published in Appl. Optics.

Susskind, J., J. Rosenfield, D. Reuter, and M. T. Chahine, 1982: The GLAS physical inversion method for analysis of HIRS/MSU sounding data. NASA Tech. Memo. TM 84936, 1-101.